MITSUBISHI ELECTRIC RESEARCH LABORATORIES
https://www.merl.com

Motion Planning for Information Acquisition via Continuous-time Successive Convexification

Uzun, Samet; Acikmese, Behcet; Di Cairano, Stefano

TR2025-170 December 10, 2025

Abstract

We address motion planning for a mobile agent to acquire information from multiple monitored tar- gets using sensors with limited capabilities. To represent sensor limitations, such as range, field of view, and allowed acquisition directions, we introduce a nonnegative metric that quantifies the rate of information acquisition and is positive only when these limitations are satisfied. To en- able optimization-based trajectory generation, we impose temporal logic specifications to ensure that the information acquisition metric and its gradient are nonzero over some time interval. This enables the application of continuous- time successive convexification to solve the motion planning problem. We demonstrate the proposed approach in a case study of a quadrotor that must acquire information on multiple targets with sensor range, field of view, and acquisition direction constraints.

IEEE Conference on Decision and Control (CDC) 2025

Mitsubishi Electric Research Laboratories, Inc.
201 Broadway, Cambridge, Massachusetts 02139

Motion Planning for Information Acquisition via Continuous-time Successive Convexification

Samet Uzun, Behçet Açıkmeşe, *Fellow, IEEE*, Stefano Di Cairano, *Fellow, IEEE*

***Abstract*— We address motion planning for a mobile agent to acquire information from multiple monitored targets using sensors with limited capabilities. To represent sensor limitations, such as range, field of view, and allowed acquisition directions, we introduce a nonnegative metric that quantifies the rate of information acquisition and is positive only when these limitations are satisfied. To enable optimization-based trajectory generation, we impose temporal logic specifications to ensure that the information acquisition metric and its gradient are nonzero over some time interval. This enables the application of continuous-time successive convexification to solve the motion planning problem. We demonstrate the proposed approach in a case study of a quadrotor that must acquire information on multiple targets with sensor range, field of view, and acquisition direction constraints.**

***Index Terms*— Autonomous systems, Perception and control, Monitoring, Numerical algorithms, Optimal control**

I. Introduction

Monitoring distributed infrastructures, such as power lines, roadways, and water networks, for preventive maintenance or tracking large-scale natural phenomena like erosion, forest overgrowth, and farmland flooding for risk mitigation is a labor-intensive, physically demanding, and potentially hazardous task. These challenges make automation technologies an ideal solution to alleviate the burden on human operators by mitigating the associated risks and difficulties [1]–[3]. Rather than dispatching people to survey impervious and faraway areas, teams of autonomous robots, e.g., drones potentially supported by ground robots acting as mobile base stations, can be deployed to gather information about monitoring targets, which can then be reviewed and analyzed for corrective actions or further investigation.

As a result, in recent years, there has been growing interest in using robots for monitoring purposes. In particular, it may be convenient to use small and inexpensive mobile robots in larger numbers as opposed to fewer, larger robots for cost, safety, and increased parallelization. Lower-cost robots, such as micro-drones, are often equipped with less capable sensors, making it crucial to consider sensor limitations and information acquisition performance when planning drone operations. For instance, considering sensor limitations like range and field of view, decisions must be made on whether to fly at a low altitude for detailed target acquisition or at a higher altitude to scan a larger area.

In prior works on automated monitoring, we have investigated the task assignment problem, i.e., dispatching drones based on current knowledge of the targets [4], [5], and the motion planning for ground robots serving as mobile stations for drone deployment and recovery [6]. Recently, there has also been an increase in the interest in perception-aware planning and control [7]–[12], but most previous works focus on limitations imposed by the information perceived about the environment rather than planning to acquire information while accounting for sensor limitations.

In this work, we address motion planning for information acquisition tasks, e.g., monitoring, while considering acquisition performance in relation to sensor limitations, including range, field of view, and target acquisition direction. We develop a smooth, non-negative information acquisition metric that quantifies the rate of information acquisition depending on the sensor limitations and performance, which takes a positive value only when all sensor limitations are satisfied. The smoothness of the proposed metric enables the application of the continuous-time successive convexification (ct-SCvx) approach to optimal control [13] where the information acquisition is enforced by continuous-time path constraints.

However, the information acquisition metric is uniformly zero beyond the sensor limitations, resulting in a uniformly zero gradient that hinders numerical optimization. Thus, we impose signal temporal logic (STL) specifications [14] to ensure that the metric and its gradient are nonzero over a specified time interval. The specifications are parameterized using generalized mean-based smooth robustness measure (GMSR) [14], resulting in a smooth and exact parameterization, which is crucial to ensuring the convergence guarantees of the ct-SCvx framework [13].

The remainder of this paper is structured as follows. Section II introduces the information acquisition metric and defines the motion planning problem for information acquisition. Section IV formulates the problem within the ct-SCvx framework, and Section V addresses its solution. Section VI demonstrates the effectiveness of our framework through a case study where a quadrotor acts as a mobile agent acquiring information from multiple monitoring targets. Finally, Section VII summarizes our findings and concludes the paper.

Notation: $\bar{x} := x/\|x\|$. $|x|_+ := \max\{0, x\}$. $|x|_- := \min\{0, x\}$. $(v_1, v_2, \dots, v_N) := [v_1^\top, v_2^\top, \dots, v_N^\top]^\top$ where v_i have arbitrary dimensions. $[1 : N] := \{1, 2, \dots, N\}$, with $N \in \mathbb{Z}_{++}$. $\mathbf{1}$ is a matrix of ones in appropriate dimensions.

S. Uzun and B. Açıkmeşe are with the Dep. Aeronautics and Astronautics, University of Washington, Seattle, WA 98105 (email:{samet, behcet}@uw.edu). S. Uzun was an intern at MERL during this work.

S. Di Cairano is with Mitsubishi Electric Research Laboratories (MERL), Cambridge, MA 02139 (email:dicairano@ieee.org).

II. Information Acquisition

We consider an agent with dynamics $\dot{x}(t) = F\big(t, x(t), u(t)\big)$ where $u \in \mathbb{R}^m$ is the input vector, $x \in \mathbb{R}^n$ is the state vector that includes position $r \in \mathbb{R}^3$, attitude $\Omega \in \mathbb{R}^3$ and possibly additional states, and the agent is subject to path constraints $g\big(t, x(t), u(t)\big) \leq 0$, $h\big(t, x(t), u(t)\big) = 0$. Given a set of targets indexed by $i \in [1\!:\!n_{\mathrm{m}}]$, we want to generate a trajectory from an initial state x_0 to a final state x_f to collect a required amount of information c_{m_i} for each target $i \in [1\!:\!n_{\mathrm{m}}]$ at position p_{m_i}.

We model the information acquired at each time instant as dependent on the target distance, the angle from which the target is observed, and the sensor field of view. Thus, we introduce a nonnegative information acquisition metric, which is a function of r and Ω, to quantify the information gathered per unit time. The metric is positive only when all of the following are satisfied: (i) the distance between the sensor and the target is less than a certain threshold, (ii) the sensor is within the acquisition cone defined by the target's position and its desired acquisition direction, and (iii) the target is within the field of view cone determined by the position and direction of the sensor. The metric increases as the sensor gets closer to the target and aligns with the centers of the information acquisition and field of view cones.

We develop an information acquisition metric to capture the instantaneous amount of acquired information. It is constructed from components $m_i : \mathbb{R}^6 \to [0, 1]$ related to the limitations of the sensor that affect the acquisition performance, see Figure 1:

1) Sensor range. Due to the distance between the agent's position and the position of the i-th target, $r, p_{\mathrm{m}_i} \in \mathbb{R}^3$,

$$m_{\mathrm{d}_i}\big(r(t)\big) := 1 + c_{\mathrm{m}_i}\left(\left(1 + e^{\tau_{\mathrm{m}_i}\rho_i(t)}\right)^{-1} - 0.5\right), \quad \text{(1a)}$$

where $\rho_i(t) := \|r(t) - p_{\mathrm{m}_i}\|$ is the distance to target i, c_{m_i} is a scaling coefficient, and τ_{m_i} is acquisition decay rate for distance.

2) Acquisition direction. Due to the directions from which a target can be successfully sensed, and based on the scaled cosine similarity between the desired acquisition direction of the i-th target, d_{m_i}, and the actual acquisition direction $\overline{\big(r(t) - p_{\mathrm{m}_i}\big)}$:

$$\tilde{m}_{\mathrm{a}_i}\big(r(t)\big) := d_{\mathrm{m}_i}^{\top}\big(\overline{r(t) - p_{\mathrm{m}_i}}\big)$$
$$m_{\mathrm{a}_i}\big(r(t)\big) := \frac{\tilde{m}_{\mathrm{a}_i}\big(r(t)\big) - \cos(\alpha_{\mathrm{a}_i}^{\mathrm{d}})}{1 - \cos(\alpha_{\mathrm{a}_i}^{\mathrm{d}})}, \quad \text{(1b)}$$

where $\alpha_{\mathrm{a}_i}^{\mathrm{d}}$ is the acquisition cone maximum angle;

3) Sensor field of view. Due to the acquisition area of the sensor and based on the scaled cosine similarity between the sensor field of view direction, $d_{\mathrm{v}}(\Omega) := \mathcal{R}(\Omega) d_{\mathrm{v}}^{\mathcal{B}}$, and the acquisition direction $\overline{\big(r(t) - p_{\mathrm{m}_i}\big)}$:

$$\tilde{m}_{\mathrm{v}_i}\big(r(t), \Omega(t)\big) := -d_{\mathrm{v}}\big(\Omega(t)\big)^{\top}\big(\overline{r(t) - p_{\mathrm{m}_i}}\big)$$
$$m_{\mathrm{v}_i}\big(r(t), \Omega(t)\big) := \frac{\tilde{m}_{\mathrm{v}_i}\big(r(t), \Omega(t)\big) - \cos(\alpha_{\mathrm{v}}^{\mathrm{d}})}{1 - \cos(\alpha_{\mathrm{v}}^{\mathrm{d}})}, \quad \text{(1c)}$$

where $\mathcal{R} : \mathbb{R}^3 \to \mathbb{R}^3$ is the rotation matrix, $d_{\mathrm{v}}^{\mathcal{B}}$ is the sensor direction in the body frame, and $\alpha_{\mathrm{v}}^{\mathrm{d}}$ is the field of view maximum angle.

Thus, the information acquired each instant increases as the range decreases, as per (1a), the smaller the angular difference between desired and actual acquisition direction (1b), and the smaller the angular difference between sensor field of view direction and acquisition direction (1c).

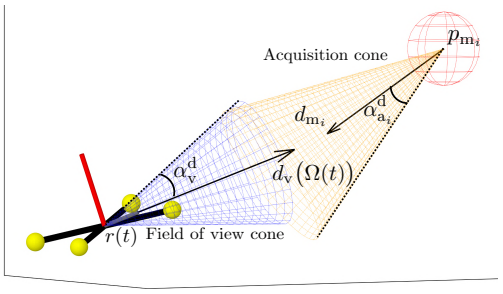

Fig. 1. Illustration of key components of the information acquisition metrics: the range, from $\boldsymbol{r}$ and $\boldsymbol{p_{\mathrm{m}_i}}$, field of view direction $\boldsymbol{d_{\mathrm{v}}(\Omega)}$ and acquisition direction, $\boldsymbol{d_{\mathrm{m}_i}}$.

With proper scaling, m_{d_i}, m_{a_i} and m_{v_i} have maximum value 1, and are 0 at the border of the corresponding sensor limitation. However, past such border, they become negative, which is not meaningful since it would indicate an increasingly negative information acquisition. Thus, we compose m_{d_i}, m_{a_i}, m_{v_i} with the $\mathcal{C}^1$-smooth function

$$q^c(x) := \left(\max(0, x)^2 + c^2\right)^{0.5} - c, \text{ where } c > 0. \quad \text{(2)}$$

Let $q^c(m_{\mathrm{j}}) = m_{\mathrm{j}}^q$, for simplicity. The resulting composed functions under-approximate the functions in (1) by an arbitrarily small number and are exactly zero beyond the sensor limitations, so that the sensors acquire no information beyond those, see Figure 2.

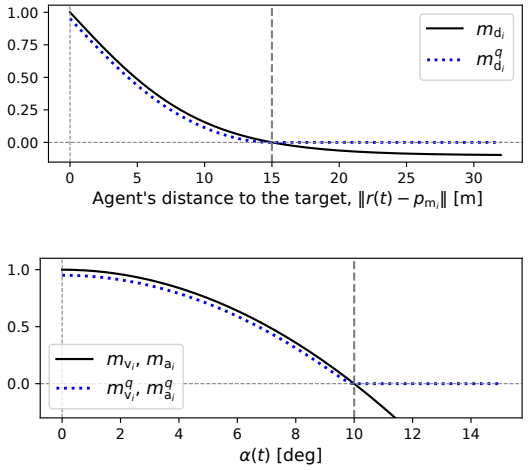

Fig. 2. Top: $\boldsymbol{m_{\mathbf{d}_i}}$ and $\boldsymbol{m^q_{\mathbf{d}_i}}$ for $\boldsymbol{c = 0.05}$, as a function of distance to the target, $\|\boldsymbol{r - p_{\mathrm{m}_i}}\|$ for $\boldsymbol{c_{\mathrm{m}_i} = 2.2}$ and $\boldsymbol{\tau_{\mathrm{m}_i} = 0.203}$. Bottom: $\boldsymbol{m_{\mathbf{a}_i}}$, $\boldsymbol{m_{\mathbf{v}_i}}$ and corresponding $\boldsymbol{m^q_{\mathbf{a}_i}}$, $\boldsymbol{m^q_{\mathbf{v}_i}}$ for $\boldsymbol{c = 0.05}$, as functions of angle $\boldsymbol{\alpha}$ for $\boldsymbol{\alpha^{\mathrm{d}}_{\mathbf{a}_i} = 10}$ deg and $\boldsymbol{\alpha^{\mathrm{d}}_{\mathbf{v}} = 10}$ deg, respectively.

Thus, we define the instantaneous information acquisition as the product of the modified components in (1a)–(1c), imposing

that information is acquired only if all the sensor limitations are satisfied, and increases as the agent's configuration away from the constraint boundaries

$$m_i\big(x(t)\big) = \bar{m}_i \cdot m^q_{\mathrm{d}_i}(r(t)) \cdot m^q_{\mathrm{a}_i}(r(t)) \cdot m^q_{\mathrm{v}_i}(r(t), \Omega(t)), \quad (3)$$

where $\bar{m}_i$ denotes the maximum achievable acquisition rate for target i, x includes the position r and the attitude Ω, and the acquired information for each target evolves as

$$\dot{z}(t) = \ m\big(x(t)\big) = \big(m_1\big(x(t)\big), \ldots, m_{n_\mathrm{m}}\big(x(t)\big)\big). \quad (4)$$

Based on (4), we want to generate a trajectory for $x(t)$, $t \in [0, t_\mathrm{f}]$ that satisfies the agent dynamics and constraints and collects a sufficient amount of information for each target,

$$z(0) = 0,$$
$$z(t_\mathrm{f}) \geq c_\mathrm{m} = \big(c_{\mathrm{m}_1}, c_{\mathrm{m}_2}, \ldots, c_{\mathrm{m}_{n_\mathrm{m}}}\big).$$

To solve such a problem, we propose an optimization-based trajectory generation approach using the ct-SCvx framework.

III. Driving Information Acquisition by STL Specifications

In regions where the sensor limitations (1) are not satisfied, $m_i(x)$ becomes uniformly zero, resulting in a null gradient that causes convergence issues in optimization-based trajectory generation. To mitigate this issue, we ensure the existence of time intervals where $m_i(x)$ and its gradient are nonzero by imposing a signal temporal logic (STL) specification [14]. First, we define the predicates

$$^{\mathrm{d}}\varphi^i := \big(f_{\mathrm{d}_i}\big(r(t)\big) \geq 0\big) := \big(r^{\mathrm{de}}_{\mathrm{d}_i} - \|r(t) - p_{\mathrm{m}_i}\| \geq 0\big), \quad (5a)$$
$$^{\mathrm{a}}\varphi^i := \big(f_{\mathrm{a}_i}\big(r(t)\big) \geq 0\big) := \big(\tilde{m}_{\mathrm{a}_i}\big(r(t)\big) - \cos(\alpha^{\mathrm{de}}_{\mathrm{a}_i}) \geq 0\big), \quad (5b)$$
$$^{\mathrm{v}}\varphi^i := \big(f_{\mathrm{v}_i}\big(r(t), \Omega(t)\big) \geq 0\big)$$
$$:= \big(\tilde{m}_{\mathrm{v}_i}\big(r(t), \Omega(t)\big) - \cos(\alpha^{\mathrm{de}}_{\mathrm{v}}) \geq 0\big), \quad (5c)$$

where $\alpha^{\mathrm{de}}_{\mathrm{a}_i} < \alpha^{\mathrm{d}}_{\mathrm{a}_i}$ and $\alpha^{\mathrm{de}}_{\mathrm{v}} < \alpha^{\mathrm{d}}_{\mathrm{v}}$. If (5a)–(5c) hold true at time t, the corresponding functions in (1a)–(1c) are nonnegative, and thus the sensing limitations are satisfied.

Second, to ensure all conditions in (5) are satisfied in a period $t_{\mathrm{E}_i} > 0$, we consider the STL specification

$$^{\mathrm{g}}\varphi^i := \boldsymbol{G}_{[0, t_{\mathrm{E}_i}]}\big(^{\mathrm{d}}\varphi^i \wedge {}^{\mathrm{a}}\varphi^i \wedge {}^{\mathrm{v}}\varphi^i\big), \quad (6)$$

where $\wedge$ denotes *conjunction*, and $\boldsymbol{G}$ is the *always* operator, which must hold over the interval $[0, t_{\mathrm{E}_i}]$. Finally, to ensure that (6) eventually holds within an interval $[t_{\mathrm{S}_i}, t_{\mathrm{S}_{i+1}}]$, where $t_{\mathrm{E}_i} \leq t_{\mathrm{S}_{i+1}} - t_{\mathrm{S}_i}$, $i \in [1\!:\!n_\mathrm{m}]$, we enforce the STL specification

$$^{\mathrm{f}}\varphi^i := \boldsymbol{F}_{[t_{\mathrm{S}_i}, t_{\mathrm{S}_{i+1}} - t_{\mathrm{E}_i}]}\, {}^{\mathrm{g}}\varphi^i, \quad (7)$$

where $\boldsymbol{F}$ is the *eventually* operator, which must hold in the time interval $[t_{\mathrm{S}_i}, t_{\mathrm{S}_{i+1}} - t_{\mathrm{E}_i}]$.

Composing "eventually" and "always" in (7) ensures that, for sufficiently small $r^{\mathrm{de}}_{\mathrm{d}_i}$ and $\alpha^{\mathrm{de}}_{\mathrm{a}_i} < \alpha^{\mathrm{d}}_{\mathrm{a}_i}$, $\alpha^{\mathrm{de}}_{\mathrm{v}} < \alpha^{\mathrm{d}}_{\mathrm{v}}$, if (7) is satisfied, there exists $t' \in [t_{\mathrm{S}_i}, t_{\mathrm{S}_{i+1}} - t_{\mathrm{E}_i}]$ such that $m_i(x)$ and its gradient are nonzero for almost every $t \in [t', t' + t_{\mathrm{E}_i}]$.

IV. Trajectory Generation by Continuous-time Successive Convexification

The trajectory generation for information acquisition is formulated as a free-final-time optimal control problem in the Mayer form, with additional constraints enforcing information acquisition and satisfaction of the STL specifications

$$\underset{x,\, u,\, t_\mathrm{f}}{\text{minimize}} \quad L\big(t_\mathrm{f}, x(t_\mathrm{f})\big) \quad (8a)$$
$$\text{subject to} \quad \dot{x}(t) = F\big(t, x(t), u(t)\big) \quad \text{a.e. } t \in [0, t_\mathrm{f}] \quad (8b)$$
$$\dot{z}(t) = m\big(x(t)\big) \quad \text{a.e. } t \in [0, t_\mathrm{f}] \quad (8c)$$
$$g\big(t, x(t), u(t)\big) \leq 0 \quad \text{a.e. } t \in [0, t_\mathrm{f}] \quad (8d)$$
$$h\big(t, x(t), u(t)\big) = 0 \quad \text{a.e. } t \in [0, t_\mathrm{f}] \quad (8e)$$
$$P\big(x(0), u(0), x(t_\mathrm{f}), u(t_\mathrm{f})\big) \leq 0 \quad (8f)$$
$$Q\big(x(0), u(0), x(t_\mathrm{f}), u(t_\mathrm{f})\big) = 0 \quad (8g)$$
$$c_\mathrm{m} - z(t_\mathrm{f}) \leq 0 \quad (8h)$$
$$z(0) = 0 \quad (8i)$$
$$\big(x(t), 0\big) \models {}^{\mathrm{f}}\varphi^i \quad \forall i \in [1\!:\!n_\mathrm{m}] \quad (8j)$$

where L is the terminal cost function, g and h are the path constraint functions, P and Q are the boundary condition constraint functions.

Methods that enforce the non-negativity of (1a)–(1c) only at discrete node points may result in insufficient data acquisition and possibly inter-sample constraint violation. In order to ensure appropriate information acquisition and constraint enforcement here we use a continuous-time successive convexification approach [13]. In the next sections, we detail the steps for solving (8) in such a framework: (IV-A) reformulate path constraints to ensure continuous-time constraint satisfaction [13]; (IV-B) transform the free-final-time problem into a fixed-final-time one via time-dilation [13]; (IV-C) parameterize the inputs to be finite-dimensional and discretize the continuous-time dynamics by multiple-shooting [15]; (IV-D) parameterize the STL specifications using the generalized mean-based smooth robustness measure (GMSR) [14].

A. Continuous-time Constraint Satisfaction

For ensuring the satisfaction of the path constraints in continuous-time [13], we remind that

$$g\big(t, x(t), u(t)\big) \leq 0, \ h\big(t, x(t), u(t)\big) = 0 \ \text{ a.e. } t \in [0, t_\mathrm{f}]$$
$$\iff \int_0^{t_\mathrm{f}} q^c\big(g\big(t, x(t), u(t)\big)\big) + q^d\big(h\big(t, x(t), u(t)\big)\big)\mathrm{d}t = 0,$$

where q^c is the same as in (2) and

$$q^d(x) := (x^2 + d^2)^{0.5} - d, \ \text{where } d > 0. \quad (9)$$

Thus, we introduce an auxiliary state y to accumulate the violation of the path constraints

$$\dot{y}(t) = \mathbf{1}^\top q^c\big(g\big(t, x(t), u(t)\big)\big) + \mathbf{1}^\top q^d\big(h\big(t, x(t), u(t)\big)\big),$$

and impose the boundary conditions:

$$y(0) = 0, \quad y(t_\mathrm{f}) = 0. \quad (10)$$

Including the cumulative constraint violation and the information acquisition, the augmented dynamics are given by

$$\begin{aligned} x_{\mathrm{a}}(t) &:= \big(x(t), y(t), z(t)\big), \\ \dot{x}_{\mathrm{a}}(t) &:= F_{\mathrm{a}}\big(t, x_{\mathrm{a}}(t), u(t)\big) \\ &:= \begin{bmatrix} F\big(t, x(t), u(t)\big) \\ \mathbf{1}^\top q^c\big(g\big(t, x(t), u(t)\big)\big) + \mathbf{1}^\top q^d\big(h\big(t, x(t), u(t)\big)\big) \\ m\big(x(t)\big) \end{bmatrix}. \end{aligned}$$

B. Time-dilation

We transform the free-final-time optimal control problem in (8) into an equivalent fixed-final-time formulation using time-dilation [13]. We define a strictly increasing, continuously differentiable function $\tilde{t} : [0,1] \to \mathbb{R}_+$ that satisfies $\tilde{t}(0) = 0$ and $\tilde{t}(1) = t_{\mathrm{f}}$. The rate of time flow, referred to as the dilation factor, is $s(\tau) := \mathrm{d}\tilde{t}(\tau)/\mathrm{d}\tau = \mathring{\tilde{t}}(\tau)$ for $\tau \in [0,1]$, where $s(\tau)$ is an additional decision variable in the optimal control problem, treated as an additional control input.

With respect to τ, derivatives are denoted as $\mathring{\square} := \mathrm{d}\square/\mathrm{d}\tau$ and state and input vectors are $\tilde{x}(\tau) := \big(x_{\mathrm{a}}(\tilde{t}(\tau)), \tilde{t}(\tau)\big)$, $\tilde{u}(\tau) := \big(u(\tilde{t}(\tau)), s(\tau)\big)$, where the additional (last) component of the state tracks time evolution, and the dilation factor is added as an input. With respect to τ, the dynamics are

$$\begin{aligned} \mathring{\tilde{x}}(\tau) &= \begin{bmatrix} \dot{x}_{\mathrm{a}}(t) \\ 1 \end{bmatrix} \frac{\mathrm{d}\tilde{t}(\tau)}{\mathrm{d}\tau} = f\big(\tilde{x}(\tau), \tilde{u}(\tau)\big) \\ &= \begin{bmatrix} F_{\mathrm{a}}\big(\tilde{t}(\tau), x_{\mathrm{a}}(\tilde{t}(\tau)), u(\tilde{t}(\tau))\big) \\ 1 \end{bmatrix} s(\tau), \end{aligned} \tag{11}$$

where now the final time is fixed, and $t_{\mathrm{f}} = \tilde{t}(1)$ is still free and dependent on the additional input s.

C. Problem Discretization

We discretize $[0,1]$ into N uniformly spaced node points $0 = \tau_1 < \cdots < \tau_N = 1$ with step size $\Delta\tau = 1/(N-1)$. The control input is parameterized by a first-order hold as $\tilde{u}(\tau) = \tilde{u}_k(\tau_{k+1} - \tau)/\Delta\tau + \tilde{u}_{k+1}(\tau - \tau_k)/\Delta\tau$ for $\tau \in [\tau_k, \tau_{k+1}]$ and $k \in [1\!:\!N-1]$.

With the state and control values at node points, x_k, u_k, $k \in \mathbb{N}$ as decision variables, we discretize the system dynamics (11) using multiple-shooting [15]

$$\tilde{x}_{k+1} = \tilde{x}_k + \int_{\tau_k}^{\tau_{k+1}} f\big(\tilde{x}^k(\tau), \tilde{u}(\tau)\big)\, \mathrm{d}\tau, \tag{12}$$

where $\tilde{x}^k(\tau)$ denotes the solution of the dynamics starting at $\tilde{x}_k$ and driven by $\tilde{u}(\tau)$. Thus, (12) is expressed as $\tilde{x}_{k+1} = f_k(\tilde{x}_k, \tilde{u}_k, \tilde{u}_{k+1})$. To avoid degenerate solutions, we impose a lower bound on the dilation factor ${}^{s}E(\tilde{u}_{k+1} - \tilde{u}_k) \geq s_{\min}$, where $s_{\min} > 0$ is the shortest time between nodes. Here, ${}^{\square}E_{\diamond}$ denotes the extraction of the $\square$-component from the vector $\diamond$. The boundary condition in (10) is relaxed to ${}^{y}E(\tilde{x}_{k+1} - \tilde{x}_k) \leq \epsilon_{\mathrm{LICQ}}$, where $\epsilon_{\mathrm{LICQ}} > 0$ is a small constant that ensures the linear independence constraint qualification [13, Sec. 3.1].

D. Parametrization of the STL specifications

Next, we parameterize the STL specification (7) using GMSR, see [14] for more details on this method. The functions for parameterizing the conjunction and disjunction operators, ${}^{\wedge}h^c_{p,w}$ and ${}^{\vee}h^c_{p,w}$, respectively, are

$$\begin{aligned} {}^{\wedge}h^c_{p,w}(a) &:= \Big(M^c_{0,w}(|a|^2_+)\Big)^{\frac{1}{2}} - \Big(M^c_{p,w}(|a|^2_-)\Big)^{\frac{1}{2}}, \\ {}^{\vee}h^c_{p,w}(a) &:= -{}^{\wedge}h^c_{p,w}(-a), \end{aligned}$$

where

$$M^c_{0,w}(b) := \Big(c^{\mathbf{1}^T w} + \prod_{i=1}^{n} b_i^{w_i}\Big)^{1/\mathbf{1}^T w}, \tag{13a}$$

$$M^c_{p,w}(b) := \Big(c^p + \frac{1}{\mathbf{1}^T w}\sum_{i=1}^{n} w_i b_i^p\Big)^{1/p}, \tag{13b}$$

$a \in \mathbb{R}^n$, $b \in \mathbb{R}^n_+$, $c \in \mathbb{R}_{++}$, $p \in \mathbb{Z}_{++}$, $w \in \mathbb{Z}^n_{++}$.

The *always* specification (6) is parameterized as

$$\begin{aligned} \Gamma^{{}^{\mathrm{g}}\varphi^i}_{\boldsymbol{c},\boldsymbol{p},\boldsymbol{w}}(\tilde{x}, k) = {}^{\wedge}h^c_{p,w}\Big(& \big({}^{\wedge}h^c_{p,w}\big(f_{\mathrm{s}_i}(r_k, \Omega_k)\big), \\ & \vdots \\ & {}^{\wedge}h^c_{p,w}\big(f_{\mathrm{s}_i}(r_{k+n_{\mathrm{E}_i}}, \Omega_{k+n_{\mathrm{E}_i}})\big)\big)\Big) \end{aligned}$$

where $f_{\mathrm{s}_i}(r_k, \Omega_k) := \big(f_{\mathrm{d}_i}(r_k), f_{\mathrm{a}_i}(r_k), f_{\mathrm{v}_i}(r_k, \Omega_k)\big)$ for $k \in [1\!:\!N]$, r_k and Ω_k denote the values of $r\big(\tilde{t}(\tau_k)\big)$ and $\Omega\big(\tilde{t}(\tau_k)\big)$, respectively, and $n_{\mathrm{E}_i} \in \mathbb{Z}_{++}$ is the number of node points required to satisfy the ${}^{\mathrm{g}}\varphi^i$ specification and chosen such that $\tilde{t}(\tau_{k+n_{\mathrm{E}_i}}) - \tilde{t}(\tau_k) \geq t_{\mathrm{E}_i}$.

The *eventually* specification (7) is parameterized as

$$\begin{aligned} \Gamma^{{}^{\mathrm{f}}\varphi^i}_{\boldsymbol{c},\boldsymbol{p},\boldsymbol{w}}(\tilde{x}, 0) = {}^{\vee}h^c_{p,w}\Big(& \big(\Gamma^{{}^{\mathrm{g}}\varphi^i}_{\boldsymbol{c},\boldsymbol{p},\boldsymbol{w}}(\tilde{x}, k_{\mathrm{S}_i}), \\ & \vdots \\ & \Gamma^{{}^{\mathrm{g}}\varphi^i}_{\boldsymbol{c},\boldsymbol{p},\boldsymbol{w}}(\tilde{x}, k_{\mathrm{S}_{i+1}} - n_{\mathrm{E}_i} - 1)\big)\Big) \end{aligned}$$

where k_{S_i} and $k_{\mathrm{S}_{i+1}}$ are the indices of the node points defining the interval $[k_{\mathrm{S}_i} : k_{\mathrm{S}_{i+1}} - 1]$, over which the ${}^{\mathrm{g}}\varphi^i$ specification must be satisfied. Since the positive side of $\Gamma^{{}^{\mathrm{f}}\varphi^i}_{\boldsymbol{c},\boldsymbol{p},\boldsymbol{w}}$ is irrelevant, we consider

$$\tilde{\Gamma}^{{}^{\mathrm{f}}\varphi^i}_{\boldsymbol{c},\boldsymbol{p},\boldsymbol{w}}(\tilde{x}, 0) \geq 0, \tag{14}$$

$$\tilde{\Gamma}^{{}^{\mathrm{f}}\varphi^i}_{\boldsymbol{c},\boldsymbol{p},\boldsymbol{w}}(\tilde{x}, 0) = \prod_{k=k_{\mathrm{S}_i}}^{k_{\mathrm{S}_{i+1}} - n_{\mathrm{E}_i} - 1} \sum_{j=0}^{n_{\mathrm{E}_i}} \Big(\mathbf{1}^\top q^c\big(f_{\mathrm{s}_i}(r_{k+j}, \Omega_{k+j})\big)\Big).$$

Constraint (14) is enforced only at the nodes. However, since $\alpha^{\mathrm{de}}_{\mathrm{a}_i} < \alpha^{\mathrm{d}}_{\mathrm{a}_i}$, $\alpha^{\mathrm{de}}_{\mathrm{v}} < \alpha^{\mathrm{d}}_{\mathrm{v}}$, the continuity of the trajectory ensures that satisfying $\tilde{\Gamma}^{{}^{\mathrm{f}}\varphi^i}_{\boldsymbol{c},\boldsymbol{p},\boldsymbol{w}}(\tilde{x}, 0) \geq 0$ for sufficiently small $r^{\mathrm{de}}_{\mathrm{d}_i}$ guarantees the existence of $t' \in [0, t_{\mathrm{f}}]$ and $\delta > 0$ such that $m_i\big(x(t)\big)$ and its gradient are nonzero almost everywhere in $(t' - \delta, t' + \delta)$, facilitating convergence of gradient-based methods.

V. Numerical Problem and Solution

The procedure detailed in Section IV results in a reformulation of the optimal control problem (8), incorporating discretized dynamics, including time-dilation, continuous-time

constraint satisfaction, parameterized control inputs, and STL specifications. We treat non-convex constraints as "soft" constraints by applying exact penalty functions, e.g., $|\cdot|_+$ and $\|\cdot\|_1$ to constraint violations [16, Chap. 17], resulting in the optimal control problem

$$\begin{aligned}
\underset{\tilde{x}_k,\,\tilde{u}_k,\,k\in[1:N]}{\text{minimize}} \quad & L\big({}^{t}E\tilde{x}_N, {}^{x}E\tilde{x}_N\big) && \text{(15a)}\\
& + w_{\text{dyn}} \sum_{k=1}^{N-1} \|\tilde{x}_{k+1} - f_k(\tilde{x}_k, \tilde{u}_k, \tilde{u}_{k+1})\|_1 \\
& + w_{\text{iq}} \big|P\big({}^{x}E\tilde{x}_1, {}^{u}E\tilde{u}_1, {}^{x}E\tilde{x}_N, {}^{u}E\tilde{u}_N\big)\big|_+ \\
& + w_{\text{eq}} \|Q\big({}^{x}E\tilde{x}_1, {}^{u}E\tilde{u}_1, {}^{x}E\tilde{x}_N, {}^{u}E\tilde{u}_N\big)\|_1 \\
& + w_{\text{stl}} \sum_{i=1}^{n_{\text{m}}} \big| - \tilde{\Gamma}^{\text{f}\,\varphi^i}_{\boldsymbol{c},\boldsymbol{p},\boldsymbol{w}}(\tilde{x}, 0)\big|_+ \\
\text{subject to} \quad & s_{\min} \le {}^{s}E(\tilde{u}_{k+1} - \tilde{u}_k) && \text{(15b)}\\
& {}^{y}E(\tilde{x}_{k+1} - \tilde{x}_k) \le \epsilon_{\text{LICQ}} && \text{(15c)}\\
& c_{\text{m}} \le {}^{z}E\tilde{x}_N && \text{(15d)}\\
& {}^{z}E\tilde{x}_1 = 0 && \text{(15e)}
\end{aligned}$$

where (15b)–(15e) are the convex constraints that do not need softening. The optimization problem in (15) is formulated as

$$\underset{Z\in\mathcal{Z}}{\text{minimize}} \;\; J_{\text{nl}}(Z) := G(Z) + w_{\text{ep}} H(C(Z)) \qquad (16)$$

where $Z = (\tilde{x}_1, \ldots, \tilde{x}_N, \tilde{u}_1, \ldots, \tilde{u}_N)$, the convex set $\mathcal{Z}$ encodes the constraints in (15b)–(15e), and convex function G and composition $H \circ C$ encode cost, penalized dynamics, boundary conditions, and parameterized STL specifications.

We solve (16) using the prox-linear method [17] that finds a stationary point of (16) by solving a sequence of convex subproblems. At iteration $j+1$, it solves

$$\begin{aligned}
&\underset{Z\in\mathcal{Z}}{\text{minimize}}\; J_{\text{lin}}(Z, Z^j, w_{\text{prox}}) := G(Z) + \qquad (17)\\
&w_{\text{ep}} H\big(C(Z^j) + \nabla C(Z^j)(Z - Z^j)\big) + \frac{w_{\text{prox}}}{2}\|Z - Z^j\|_2^2,
\end{aligned}$$

where Z^j is the previous iterate. With a suitably chosen proximal weight w_{prox}, the sequence Z^j converges, and if the limit point is feasible for the hard constrained discretized optimal control problem, it satisfies the KKT conditions. Here, we adopt the adaptive weight update strategy from [18, Alg. 2.2] to determine w_{prox}.

VI. Case Study: Monitoring Drone

We demonstrate the approach in a case study where a drone needs to acquire information about 6 targets with desired information levels c_{m_i}, $i = [1{:}6]$. We consider a small quadrotor drone with mass $m = 1$ kg and principal moments of inertia about the body frame axes $(I_x, I_y, I_z) = (0.07, 0.07, 0.127)$ kg m^2. We model its motion by the 6-DoF translational and rotational Euler-Lagrange dynamics, where (r_x, r_y, r_z) is the position vector in the inertial frame, (v_x, v_y, v_z) is the velocity vector in the body frame, ϕ, θ, ψ are the roll, pitch, and yaw angles, and p, q, r the corresponding angular rates. The control inputs are thrust T and torques τ_ϕ, τ_θ, τ_ψ in the body-frame axes. The angular rates, pitch and roll angles, altitude, velocity, thrust, and torques are subject to bounds, and the distance from the targets must be at least 1.5 m to avoid collisions.

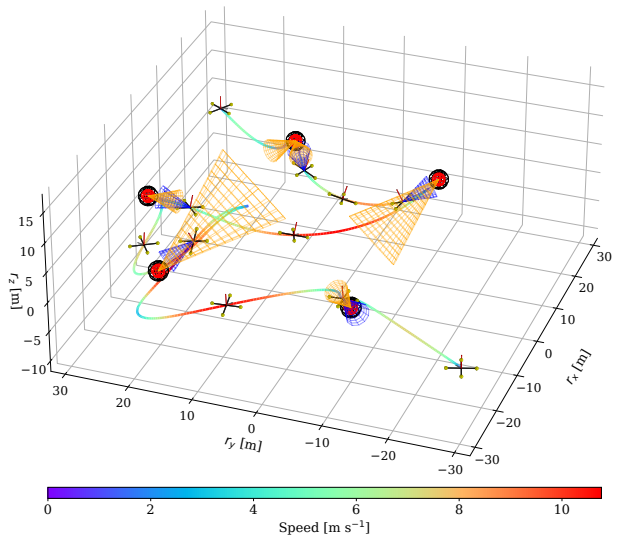

Fig. 3. Trajectory generation for a quadrotor acquiring information from 6 targets. The trajectory color represents velocity, as indicated by the colorbar below the plot. Snapshots show the quadrotor at different time instants, with targets (red spheres), collision areas (black spheres), acquisition cones (yellow cones), and sensor fields of view during information acquisition (blue cones).

Vector	Value
d_{m}	$\begin{bmatrix} \frac{1}{\sqrt{2}} & \frac{1}{\sqrt{3}} & 0 & -\frac{1}{\sqrt{3}} & -\frac{\sqrt{3}}{2} & -\frac{\sqrt{3}}{2} \\ \frac{1}{\sqrt{2}} & -\frac{1}{\sqrt{3}} & -1 & \frac{1}{\sqrt{3}} & -\frac{1}{2} & \frac{1}{2} \\ 0 & \frac{1}{\sqrt{3}} & 0 & -\frac{1}{\sqrt{3}} & 0 & 0 \end{bmatrix}$

TABLE I
Matrix of the acquisition directions for the different targets, as columns

We account for range (1a) and field of view (1c) limitations on the sensor and acquisition cone constraints (1b) on the targets, where $c_{\text{m}_i} = 2.2$, $i \in [1:6]$, $\tau_{\text{m}} = (0.223,\ 0.063,\ 0.223,\ 0.085,\ 0.223,\ 0.223)$, $\alpha^{\text{d}}_{\text{v}} = 20$ deg, $\alpha^{\text{d}}_{\text{a}_i} = 20$ deg, $i \in [1{:}6]$, $\bar{m}_i = 0.38$, $i \in [1{:}6]$. The acquisition cones have orientation d_{m_i} in the (x, y) plane for some targets and angled for others, see Table I. Here, the sequence of targets is pre-assigned, e.g., from the algorithm in [4].

We implement the STL specification (7) where $r^{\text{de}}_{\text{d}} = (6,\ 20,\ 6,\ 15,\ 6,\ 6)$ m, $\alpha^{\text{de}}_{\text{v}} = 15$ deg, $\alpha^{\text{de}}_{\text{a}_i} = 15$ deg, $i \in [1{:}6]$, and $k_{\text{S}} = (1,\ 16,\ 25,\ 36,\ 45,\ 50,\ 61)$, $n_{\text{E}_i} = 3$, $i \in [1{:}6]$. In (2) and (9), $c = d = 10^{-4}$ to ensure smoothness with a negligible impact on the numerical algorithm.

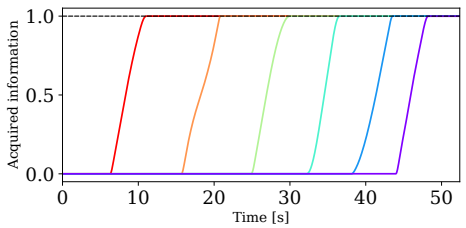

Fig. 4. History of information acquired during the quadrotor flight for each target, from red (first target) to purple (last target).

For given boundary conditions, we use $K = 61$ node

points with the flight time treated as a decision variable to be minimized. We initialize the optimization with a trajectory composed of straight lines connecting the initial position to the sequence of targets and then to the final position. Node points are distributed uniformly along the trajectory. We also apply affine scaling to the optimization problem parameters to improve the numerical conditioning. We implement (17) using CVXPY [19] and CLARABEL [20] solver.

Figure 3 shows the scenario of the simulation[1], and Figures 4, 5 show the information acquisition history for each target and the state and control variables. The quadrotor acquires the required information for each target in less than 51s and satisfies the state and input constraints continuously during the flight. For comparison, a conventional method that decouples motion planning and information acquisition—where the agent repeatedly flies to a point, stops to acquire information, then proceeds to the next—results in a total mission time of 66.17s, comprising 42.31s for motion and 23.86s for acquisition. This is approximately 29% longer than our proposed approach. Also, if the sensor field of view and acquisition direction cones are too narrow, the baseline may fail for targets with steeply tilted acquisition directions, as acquisition requires the drone to pitch, which prevents the flight from being stationary.

The trajectory computation in a simple, non-optimized Python implementation of the method takes approximately 14.5s on a 2023 MacBook Pro. Speedups of $10\times - 40\times$ are expected by code optimization, compilation, and conversion to C/C++. Thus, even if the proposed approach is primarily for offline trajectory generation, a receding horizon implementation with a shorter time window and fewer nodes may achieve real-time operation.

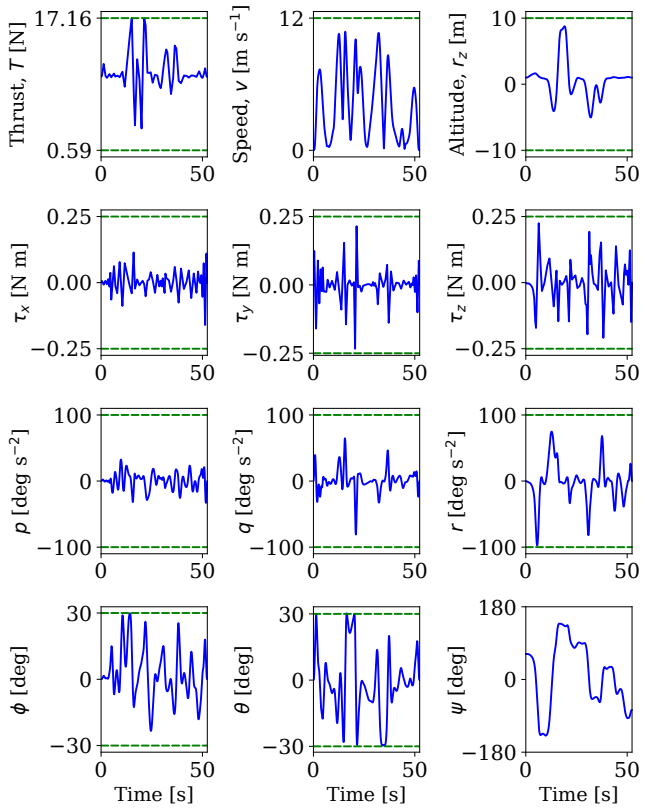

Fig. 5. History of state and control variables during the quadrotor flight (blue solid) and constraints (green dash).

VII. Conclusions

We developed motion planning for a mobile agent to acquire information while accounting for sensor limitations. We introduced an information acquisition metric and imposed path constraints in a continuous-time successive convexification approach ensuring sufficient information is acquired on each target. To facilitate numerical convergence, we imposed STL specifications ensuring that the cost function gradient is nonzero in some time interval. In the future, we will consider acquisition over distributed areas and controllable sensors.

References

[1] M. Dunbabin and L. Marques, "Robots for environmental monitoring: Significant advancements and applications," *IEEE Robotics & Automation Mag.*, vol. 19, no. 1, pp. 24–39, 2012.

[2] J. Zhang, J. Hu, J. Lian, Z. Fan, X. Ouyang, and W. Ye, "Seeing the forest from drones: Testing the potential of lightweight drones as a tool for long-term forest monitoring," *Biological Conserv.*, 2016.

[3] F. Flammini, C. Pragliola, and G. Smarra, "Railway infrastructure monitoring by drones," in *Int. Transp. Electr. Conf.*, 2016.

[4] P. Thaker, S. Di Cairano, and A. P. Vinod, "Bandit-based multi-agent search under noisy observations," in *Proc. IFAC World Congress*, 2023.

[5] X. Lin, S. Nayak, S. Di Cairano, and A. P. Vinod, "Data-driven spatial classification using multi-arm bandits for monitoring with energy-constrained mobile robots," *arXiv preprint arXiv:2501.08222*, 2025.

[6] T. Kim, A. P. Vinod, and S. Di Cairano, "Decoupled trajectory planning for monitoring UAVs and UGV carrier by reachable sets," in *American Control Conf.*, 2024, pp. 587–593.

[7] D. Falanga, P. Foehn, P. Lu, and D. Scaramuzza, "PAMPC: Perception-aware model predictive control for quadrotors," in *IEEE/RSJ Int. Conf. Intell. Robots and Systems*, 2018.

[8] P. Salaris, M. Cognetti, R. Spica, and P. R. Giordano, "Online optimal perception-aware trajectory generation," *IEEE Trans. Robotics*, vol. 35, no. 6, pp. 1307–1322, 2019.

[9] J. Tordesillas and J. P. How, "Panther: Perception-aware trajectory planner in dynamic environments," *IEEE Access*, 2022.

[10] M. Greeff, T. D. Barfoot, and A. P. Schoellig, "A perception-aware flatness-based model predictive controller for fast vision-based multi-rotor flight," *IFAC-PapersOnLine*, vol. 53, no. 2, pp. 9412–9419, 2020.

[11] A. Suresh and S. Martínez, "Risk-perception-aware control design under dynamic spatial risks," *IEEE Control Sys. Lett.*, 2021.

[12] A. D. Bonzanini, A. Mesbah, and S. Di Cairano, "Perception-aware model predictive control for constrained control in unknown environments," *Automatica*, vol. 160, p. 111418, 2024.

[13] P. Elango, D. Luo, A. G. Kamath, S. Uzun, T. Kim, and B. Açıkmeşe, "Successive convexification for trajectory optimization with continuous-time constraint satisfaction," *preprint arXiv:2404.16826*, 2024.

[14] S. Uzun, P. Elango, P.-L. Garoche, and B. Açıkmeşe, "Optimization with temporal and logical specifications via generalized mean-based smooth robustness measures," *arXiv preprint arXiv:2405.10996*, 2024.

[15] H. G. Bock and K. J. Plitt, "A multiple shooting algorithm for direct solution of optimal control problems," *IFAC Proceedings Volumes*, vol. 17, no. 2, pp. 1603–1608, Jul. 1984.

[16] J. Nocedal and S. Wright, *Numerical Optimization*. Springer, 2006.

[17] D. Drusvyatskiy and C. Paquette, "Efficiency of minimizing compositions of convex functions and smooth maps," *Math. Programm.*, 2019.

[18] C. Cartis, N. I. Gould, and P. L. Toint, "On the evaluation complexity of composite function minimization with applications to nonconvex nonlinear programming," *SIAM J. Optimization*, 2011.

[19] S. Diamond and S. Boyd, "CVXPY: A python-embedded modeling language for convex optimization," *Journal of Machine Learning Research*, vol. 17, no. 83, pp. 1–5, 2016.

[20] P. J. Goulart and Y. Chen, "Clarabel: An interior-point solver for conic programs with quadratic objectives," *arXiv:2405.12762*, 2024.

[1] Animation available at: https://youtu.be/DfcOXTj7gfE